Evidence of a Hardening in the Cosmic Ray Proton Spectrum at around 166 TeV Observed by the GRAPES-3 Experiment

F. Varsi,[1] S. Ahmad,[2] M. Chakraborty,[3] A. Chandra,[2] S. R. Dugad,[3] U. D. Goswami,[4] S. K. Gupta,[3] B. Hariharan,[3] Y. Hayashi,[5] P. Jagadeesan,[3] A. Jain,[3] P. Jain,[1] S. Kawakami,[5] H. Kojima,[6] P. Lipari,[7] S. Mahapatra,[8] P. K. Mohanty[3,*] R. Moharana,[9] Y. Muraki,[10] P. K. Nayak,[3] T. Nonaka,[11] A. Oshima,[6] B. P. Pant,[9] D. Pattanaik,[3,8] S. Paul,[3] G. S. Pradhan,[12] M. Rameez,[3] K. Ramesh,[3] L. V. Reddy,[3] S. Saha,[1] R. Sahoo,[12] R. Scaria,[12] S. Shibata,[6] and M. Zuberi[3]

(GRAPES-3 Collaboration)

[1]*Indian Institute of Technology Kanpur, Kanpur 208016, India*
[2]*Aligarh Muslim University, Aligarh 202002, India*
[3]*Tata Institute of Fundamental Research, Homi Bhabha Road, Mumbai 400005, India*
[4]*Dibrugarh University, Dibrugarh 786004, India*
[5]*Graduate School of Science, Osaka Metropolitan University, Sugimoto, Sumiyoshi, Osaka 558-8585, Japan*
[6]*College of Engineering, Chubu University, Kasugai, Aichi 487-8501, Japan*
[7]*INFN, Sezione Roma "Sapienza", Piazzale Aldo Moro 2, 00185 Roma, Italy*
[8]*Utkal University, Bhubaneswar 751004, India*
[9]*Indian Institute of Technology Jodhpur, Jodhpur 342037, India*
[10]*Institute for Space-Earth Environmental Research, Nagoya University, Nagoya 464-8601, Japan*
[11]*Institute for Cosmic Ray Research, Tokyo University, Kashiwa, Chiba 277-8582, Japan*
[12]*Indian Institute of Technology Indore, Indore 453552, India*

We present the measurement of the cosmic ray proton spectrum from 50 TeV to 1.3 PeV using 7.81×10^6 extensive air shower events recorded by the ground-based GRAPES-3 experiment between 1 January 2014 and 26 October 2015 with a live time of 460 day. Our measurements provide an overlap with direct observations by satellite and balloon-based experiments. The electromagnetic and muon components in the shower were measured by a dense array of plastic scintillator detectors and a tracking muon telescope, respectively. The relative composition of the proton primary from the air shower data containing all primary particles was extracted using the multiplicity distribution of muons which is a sensitive observable for mass composition. The observed proton spectrum suggests a spectral hardening at $\sim$166 TeV and disfavors a single power law description of the spectrum up to the Knee energy ($\sim$3 PeV).

Introduction.—Earth's atmosphere is continuously bombarded by high energy charged particles from space known as cosmic rays (CRs), with mass composition starting from proton (H), helium (He) to heavier nuclei such as nitrogen (N), aluminium (Al), and iron (Fe) [1]. Our knowledge of their origin, acceleration mechanism inside the source, and propagation in the interstellar medium is still limited. Hence this is still an active and fascinating area of research. The CR energy spectrum follows a nonthermal power law over its existing energy range of 10^8–10^{20} eV with distinct long-known features, the Knee (at $\sim 3 \times 10^{15}$ eV), Ankle (at $\sim 4 \times 10^{18}$ eV), and GZK cutoff (at $\sim 5 \times 10^{19}$ eV) [2–6]. Although it is believed to follow a single power law up to the Knee energy, the recent direct measurements of CRs suggest additional features like hardening at several hundred GeV [7–10] and softening at $\sim$10 TeV [9–12] in the proton spectrum which is contrary to that long-held belief. Notably, the extrapolation of these direct measurements up to the Knee does not uniquely match the extensive air shower (EAS) measurements on the ground, where an unfolding procedure is used to model the cosmic ray showers in the atmosphere [13]. This observation motivates proposals that more than one population of supernova remnants (SNRs) may be contributing to the CR spectrum at different energies [14,15].

Study of CRs above 100 TeV relies on ground-based EAS observations as the direct observations lack statistics due to the small detector area despite their excellent energy and mass resolution capabilities. The GRAPES-3, located in Ooty, India (11.4 °N, 76.7 °E, 2200 m altitude) is an
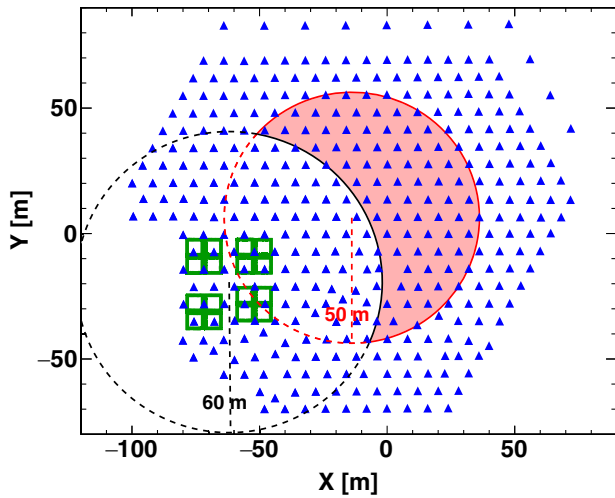
051002-1

FIG. 1. A schematic of GRAPES-3 detector components showing plastic scintillator detectors (shaded triangle), muon telescope consisting of 16 modules (square). The red and black circles represent the selection cuts on the reconstructed EAS cores (see text for details). The red-filled area represents the fiducial area for this analysis.

EAS experiment, designed with a high-density array of 400 plastic scintillator detectors (SDs) with an inter-detector separation of 8 m which is spread over an area of 25 000 m^2 [16,17]. Thus, it achieves a low energy threshold of well below 100 TeV, giving an overlapping measurement with direct experiments. Further, it is equipped with a 560 m^2 area tracking muon telescope (G3MT), consisting of 3712 proportional counters (PRCs) to measure the muon component in EAS, which is a sensitive observable for the mass composition [18]. In this Letter, we present the results of the cosmic ray proton spectrum from 50 TeV to 1.3 PeV, extracted using the muon multiplicity distributions (MMDs), and highlight a new feature observed for the first time between 100 and 200 TeV.

EAS reconstruction.—As shown in Fig. 1, the SDs measure charged particle densities in the EAS, including electrons and muons, and their relative arrival times. The EAS trigger is generated by the SD array. The EAS parameters such as core location (X_c, Y_c), shower size (N_e), and age (s), were obtained by fitting the Nishimura-Kamata-Greisen (NKG) function [19,20] to the observed particle densities [21] and its angle (θ, ϕ) was determined with a plane fit to the observed relative arrival times [22]. The G3MT is designed to record muons of energy > 1 GeV associated with the EAS by absorbing the electromagnetic component through a shield of concrete absorber of 550 $g\,cm^{-2}$. The muons in an EAS are counted after reconstructing their tracks in PRC layers along (θ, ϕ) of the EAS obtained from the SD data [23].

MC simulations.—CR primaries including H, He, N, Al, and Fe were simulated using the CORSIKA [24] package of version 7.6900 to generate EAS at the GRAPES-3 location. Post-LHC QGSJET-II-04 [25] and FLUKA [26] hadronic interaction generators were used above and below 80 GeV, respectively. Elements N, Al, and Fe represent the light (C, N, O), medium (Mg, Al, Si), and heavy (Mn, Fe, Co) mass groups in the PCRs. A total of 6.1×10^7 EAS were simulated in the energy range of 1 TeV to 10 PeV per particle for each primary in 20 equal width logarithmic bins with spectral index of -2.5 (see Sec. 3.1 of [23] for details). A single spectrum from 1 TeV to 10 PeV was produced from the pregenerated 20 bins using a spectral index of -2.7 by appropriately weighting the event contents of each bin. Each EAS was reused 10 times with a random core location in a circular area of radius 150 m from the center of the array (-13.9 m, 6.3 m) (set-1). A similar spectrum was generated from 100 TeV to 10 PeV to improve the statistics at higher energy (set-2). Each EAS in set-2 was randomly thrown ten times in a circular area of radius 60 m from the center of the array instead of 150 m radius used for set-1 data which further increased the statistics of events (by a factor of 6.25). We could make this choice considering the EAS core selection area for the analysis to be 50 m from the center of the array and taking advantage of the good core resolution at higher energy ($\sim$3 m at 100 TeV, which improves to $\sim$0.5 m at 1 PeV). The response of the G3MT to all the particles, including electrons, gamma rays, muons, and hadrons, were simulated using the GEANT4 package [27], and muon tracks were reconstructed for each triggered EAS [23]. To estimate various systematic and quality checks for the unfolding procedure, the MC simulations with spectral features proposed by two well-known cosmic ray composition models, namely, Gaisser-Stanev-Tilav (GST) [15] and H4a [28], were used.

Dataset and selection cuts.—For this analysis, the data recorded by the SD array from 1 January 2014 to 26 October 2015 were used which comprised 1.75×10^9 EASs. The same set of selection cuts was applied to ensure that both the observed and the MC simulation reconstructed datasets were treated identically. The value of s was confined between 0.02 and 1.98 to avoid poorly reconstructed EASs, converging to their limits [0, 2]. The reconstructed showers were selected with core within 50 m radius from the center of the array represented by the red circle in Fig. 1. This is to limit the contamination of mis-reconstructed EASs to < 1% due to the core landing near the edge or outside the array. Further, EAS cores landing beyond 60 m radius from the center of the G3MT as represented by the black circle in Fig. 1, but within the red circle area were selected to minimize the hadron punch-through contribution to < 2% [23]. The θ was selected below 17.8° to minimize the systematics caused by the inclined events. To reduce the systematics caused by low trigger efficiency, $N_e > 10^4$ was used, which ensured >90% trigger efficiency. Additionally, the daily observed

N_e spectrum was manually compared with the average monthly spectrum. The days in which it deviated by more than $\pm 2\%$ where one standard deviation statistical fluctuation is $\sim 0.62\%$ or showed a systematically increasing or decreasing trend were excluded from the analysis. Abnormalities in the associated electronics channels or data acquisition system caused this problem. After applying all the selection cuts, the surviving EASs were 7.81×10^6, with a live time (T_{live}) of 3.97×10^7 s (~ 460 day). The number and percentage of observed EASs surviving after each quality cut are listed in the second and third columns of Table S7 of the Supplemental Material [29]).

Analysis.—The sensitivity of MMDs to the nature of CRs has already been reported [18,21,33]. Here the observed MMD along with N_e was used to extract the relative composition of the proton and other contributing primaries using an unfolding procedure. The same procedure was applied to measure the energy distribution of proton primaries from a subset of the observed N_e distribution obtained by using the relative contribution of protons.

(i) Generating MMDs.—Although arrival time spread of muons in the EAS is several nanoseconds, the actual measured arrival time is several microseconds due to the slow response of the PRCs. A time window of 3.84 μs around the EAS trigger arrival time was used to reduce the contribution of muons that are not associated with EAS. A further reduction in the unassociated muon contribution was achieved by limiting the bottom PRC layer's search space to ± 1 PRC (equivalent to $10°$ for near vertical EAS) along the projection of the EAS direction during the track reconstruction [23]. Such a selection was allowed as it was inferred from the MC simulations that the angular distribution of muons around the EAS direction for the GRAPES-3 geometry has a standard deviation of $\sim 3°$. The above two criteria resulted in the unassociated muon contributions to 0.1 tracks per EAS. This irreducible contribution was corrected by adding an equivalent number of random tracks in the MC simulations.

The muon multiplicity was corrected for the track saturation effect for both the observed data and MC simulations [23]. The normalized MMDs for the observed data, and each simulated primary were generated by applying all selection cuts for N_e bins from $10^{4.0}$ to $10^{6.0}$ of bin-width 0.2 on a logarithmic scale. The parametrization of MMDs is discussed in S2.B of the Supplemental Material [29].

(ii) Extraction of relative composition of CRs.—The relative composition of the assumed five primary masses (H, He, N, Al, and Fe) was extracted for each N_e bin separately (see S3 of the Supplemental Material [29]). The observed MMD of a given N_e bin is a convoluted distribution of different primaries. It was deconvoluted using Gold's unfolding algorithm [34] which is an iterative method, and the algorithm's convergence is equivalent to the chi-square minimization. The required response matrix
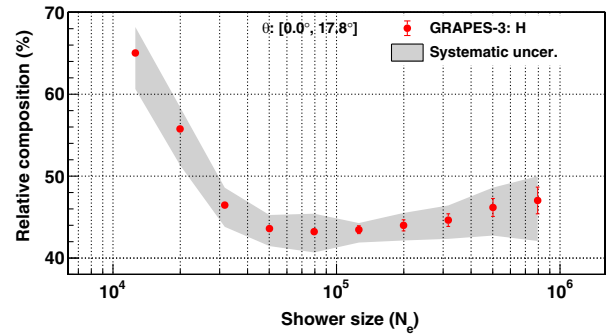

FIG. 2. Relative composition of proton primaries obtained using Gold's unfolding for GRAPES-3 data as a function of shower size. The error bar represents statistical uncertainty, and the gray band represents the total systematic uncertainty.

$\mathbf{R_1}$ that contains the relationship between the true mass and the reconstructed muon multiplicity was generated from the MC data. The elements of the response matrix $R_{1,\alpha i}$ represents the probability of an EAS initiated by the ith simulated primary having the muon multiplicity value α for a given N_e. The relative composition proposed by the GST model was used for the initial guess. The final composition was cross-checked with an initial guess from the H4a model and uniform composition (see S3.D.ii of the Supplemental Material [29]), and the relative deviation was included as the systematic uncertainty. Figure 2 shows the relative composition of proton primaries for the GRAPES-3 data. The relative composition is 65% at $N_e = 10^{4.1}$, decreasing rapidly for the two succeeding N_e bins. It is followed by a gradual increase to 47% at $N_e = 10^{5.9}$. The error bar and gray band represent the statistical and total systematic uncertainty, respectively. The statistical uncertainty increases from 0.3% to 3.5% for N_e range $10^{4.1}$–$10^{5.9}$. The total systematic uncertainty is $+4.9\%/-6.8\%$ at $N_e = 10^{4.1}$ and increased to $+6.3\%/-10.5\%$ at $N_e = 10^{5.9}$. The significant contributions to systematic uncertainty come from limited statistics of MC simulations and the use of simulated spectra with different spectral profiles to generate the response matrix. The details on estimating the systematic uncertainties due to various sources are mentioned in S3.D of the Supplemental Material [29]. Furthermore, Bayesian unfolding [35] was used to validate the final results and calculate the systematic uncertainty due to the unfolding algorithm (see S3.D.i of the Supplemental Material [29]). A MC simulation was carried with known composition of the five assumed primaries to test the reliability of the composition extraction for different primaries. Among all the primaries, the proton composition was reproduced quite well which could be possibly due to the dominant abundance of proton at low energy. We present the composition of proton in this Letter and that of heavier primary masses will be presented in a future paper after further studies.

(iii) Proton energy spectrum.—The proton energy distribution (E) was obtained using a response matrix ($\mathbf{R_2}$) which contains the relationship between the true energy and reconstructed size, convoluted with the effects of the fluctuations of the shower development, trigger and reconstruction efficiencies, and detector response. The proton MC data with a spectral slope of -2.7 were used to generate $\mathbf{R_2}$. From the observed size distribution (N_e), a size distribution (N_{e1}) for the proton primary was obtained by weighting the number of EASs in each bin of it with the relative proton composition value of the corresponding bin as presented in Fig. 2. N_{e1} was deconvoluted using $\mathbf{R_2}$ and Gold's unfolding algorithm to obtain the proton energy spectrum. The $R_{2,\alpha i}$ element of $\mathbf{R_2}$ represents the probability that a proton-initiated EAS belonging to ith energy bin is reconstructed in α^{th} size bin (see Fig. S11 of Supplemental Material [29]). The initial guess for energy was selected with a spectral hardening near 200 TeV for faster convergence. However, different initial guesses were used to verify the final energy distribution and treated as a source of systematic uncertainty. Smoothing was applied after each iteration to control the statistical fluctuations (especially at higher energies) using the 353HQ-twice algorithm [36] from the ROOT package [37]. However, the final unfolded energy distribution was not smoothed. The same criterion of minimum WMSE was used to stop the unfolding iterations.

The shower size and energy distributions belong to reconstructed and true parameter phase spaces, respectively. Some EAS, especially with shower core and direction near the boundary of selection cuts, belonging to energy distribution may not present in size distribution due to the finite core and angular resolution, called a miss EAS, and vice versa, is called a fake EAS. These transfer effects are not symmetric in reconstructed and true parameter phase spaces. Thus, correction factors for these transfers were calculated with MC simulations and applied to data in the respective phase spaces (see S5.B of the Supplemental Material [29]).

After the unfolded energy distribution for the proton primary was estimated, the value of differential flux $\Phi(E_i)$ for the ith energy bin was calculated from

$$\Phi(E_i) = \frac{1}{T_{\text{live}}}\left(\frac{n(E_i)}{\Delta E_i \cdot A_\Omega(E_i)}\right), \qquad (1)$$

where T_{live} is the live time of the observed data for this analysis, $n(E_i)$ and ΔE_i are the number of EASs and bin width of the ith energy bin, respectively, and $A_\Omega(E_i)$ is the acceptance of the GRAPES-3 SD array in the same energy bin. $A_\Omega(E_i)$ was determined by the product of the effective area of the SD array and the viewing solid angle, and calculated using,

$$A_\Omega(E_i) = \pi a \varepsilon_{\text{tot}}(E_i)(\cos^2\theta_l - \cos^2\theta_u), \qquad (2)$$

where $a = 4123$ m^2 is the fiducial area represented by the red filled area in Fig. 1, $[\theta_l, \theta_u] = [0°, 17.8°]$ is the zenith angle range used in this analysis, and ε_{tot} is the total efficiency which was estimated with the aid of MC simulations as the fraction of the EASs landing in the fiducial area that generates the trigger and passes all the selection cuts. The statistical fluctuations in the acceptance were modeled with the Richards function in the energy region where the trigger efficiency was greater than 75%. The Richards function $[f_R(E)]$ is given as

$$f_R(E) = \frac{C}{(1 + (2^\nu - 1)e^{-\alpha(\log(E/\text{GeV})-\mu)})^{\frac{1}{\nu}}}, \qquad (3)$$

where C, ν, α, and μ are the fit parameters. The Richards function reduces to the error function for $\nu = 1$. The value of fit parameters obtained from fitting is C $= 1196.6$ m^2 sr, $\nu = 3.1$, $\alpha = 7.3$, and $\mu = 4.3$ for proton primary. The uncertainties in fit parameters were used to estimate the systematic uncertainty in the acceptance. The top panel of Fig. 3 shows the energy spectrum of proton primary measured with the GRAPES-3 data from this analysis, along with the corresponding statistical and systematic uncertainties represented by error bars and the gray band, respectively. Each data point in the plot corresponds to the geometric mean energy, which is 50.1 TeV for the first point and 1.3 PeV for the last point. The energy resolution
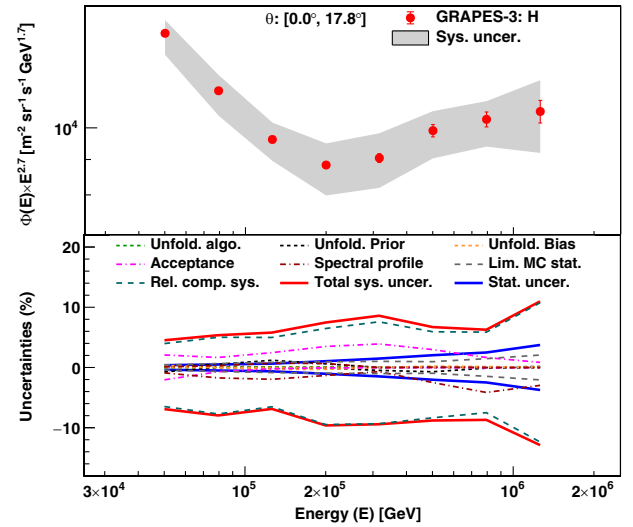

FIG. 3. Top: The proton energy spectrum measured with the GRAPES-3 data. The spectrum is scaled with E$^{2.7}$ to show the hardening of the spectrum near 166 TeV. The red error bars and the gray band represent the statistical and total systematic uncertainty, respectively. Bottom: The statistical (thick blue line) and total systematic uncertainty (thick red line), calculated by adding the contribution of systematic uncertainty from different sources in quadrature, as a function of primary energy. Dashed lines with different colors represent the contribution from different sources of systematic uncertainty.

at these two points is ~60% and ~35% (details in S4 of the Supplemental Material [29]). The $\Phi(E)$ was scaled with $E^{2.7}$ for clear visibility of the spectral features. The statistical uncertainty increases from 0.4% at 50.1 TeV to 3.7% at 1.3 PeV.

The contribution to systematic uncertainties from various sources, including acceptance, limited MC statistics, unfolding, and spectra with different spectral features to generate $\mathbf{R_2}$, was estimated and shown in the bottom panel of Fig. 3. The total systematic uncertainty was calculated by adding the contribution of systematic uncertainty from different sources in quadrature. It increases from $+4.5\%/-6.9\%$ to $+11.0\%/-12.9\%$ for the energy range of 50.1 TeV to 1.3 PeV. The systematic uncertainty in the relative composition of proton primaries was iteratively propagated to unfolded energy distribution, which is the dominant contributor to total systematic uncertainty (see S5.E of the Supplemental Material [29]).

Discussion and conclusion.—Figure 4 shows a comparison of the proton energy spectrum measured from GRAPES-3 data using Gold's unfolding algorithm and the post-LHC QGSJET-II-04 hadronic interaction model with the results from balloon or satellite observations including ATIC-2 [38], CREAM-I + III [39], NUCLEON KLEM [12], DAMPE [9], CALET [10], and ISS-CREAM [11], and air shower observations including KASCADE [2,40] and IceTop [41]. The GRAPES-3 measurement is in good agreement with the ISS-CREAM observations in an energy range from 80 to 500 TeV (the last point of the ISS-CREAM observation) within the statistical uncertainty. The measurements agree well with the CREAM-I-III observations at the lower energy side, especially in the energy range from 100 to 250 TeV. There is a good agreement with DAMPE within systematic error at 80 TeV. The first data point for GRAPES-3 measurement has a relatively higher flux than DAMPE, CREAM-III, ISS-CREAM, and CALET but is lower than the NUCLEON KLEM
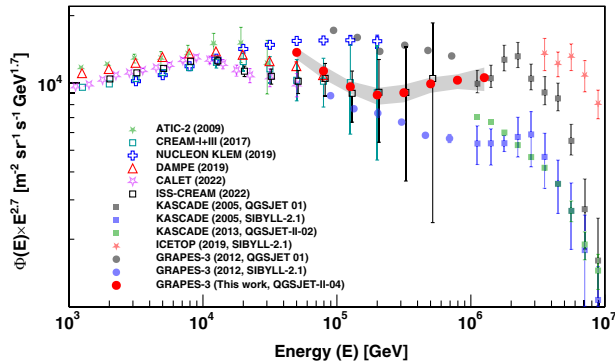

FIG. 4. Cosmic ray proton energy spectrum measured with the GRAPES-3 data (red circles) compared with results from direct and indirect observations (see text for references). The statistical error bars are smaller than the marker size and the gray band represents systematic uncertainty.

observation. On the higher energy side, the GRAPES-3 measurement shows good agreement with the KASCADE QGSTJET 01 within the statistical uncertainties. However, this measurement exhibits a systematically higher flux than the KASCADE SIBYLL-2.1 and KASCADE QGSJET-II-02. The current results are also significantly different from the earlier results of GRAPES-3 obtained using SIBYLL-2.1 and QGSJET 01 hadronic interaction models [21]. It is to be noted that the SIBYLL-2.1, QGSJET 01, and QGSJET-II-02 are pre-LHC models where significant difference in the muon production is observed among the models. However, the post-LHC models show only a few percent difference in the muon number. But the difference is 20%–50% as compared to the pre-LHC model SIBYLL-2.1 as discussed in Ref. [42].

A spectral break is observed between 100 and 200 TeV. The earlier analyses did not reveal this feature where a Gaussian method was used [21,33]. The observed N_e distribution is subject to systematic smearing under the influence of inherent fluctuations in the EAS development, detector resolution, trigger, and reconstruction efficiencies. The unfolding method is used to address this issue. To assess the effectiveness of the unfolding in contrast to the Gaussian method, we carried out a simulation test with a known input spectrum (details in S8 of the Supplemental Material [29]). We observed that the unfolding method reproduces the input spectrum unlike the Gaussian method which shows a dependency on the chosen spectral profile for the EAS simulation.

The significance of the spectral break was studied by comparing the fit results from a single power law (PL) with a spectral index (γ) of form,

$$\Phi_{PL}(E) = \Phi_0 \left(\frac{E}{50 \text{ TeV}}\right)^\gamma, \qquad (4)$$

where Φ_0 is the flux normalization constant at 50 TeV and a smoothly broken power law (SBPL) of form

$$\Phi_{SBPL}(E) = \Phi_0 \left(\frac{E}{50 \text{ TeV}}\right)^{\gamma_1} \left[1 + \left(\frac{E}{E_b}\right)^{\frac{1}{w}}\right]^{(\gamma_2-\gamma_1)w}, \qquad (5)$$

where E_b is the energy corresponding to the position of spectral break, γ_1 and γ_2 are the spectral indices before and after the spectral break, and w is the smoothness parameter for the spectral break. Figure 5 shows the fit results of the GRAPES-3 proton spectrum with the blue dashed line representing the PL function and the black line representing the SBPL function. It can be noted that only statistical uncertainties have been considered in this fit. The fit parameters are $\Phi_0 = (2.70 \pm 0.01) \times 10^{-9}$ m^{-2} sr^{-1} s^{-1} GeV^{-1} and $\gamma = -2.95 \pm 0.01$ with $\chi^2_{PL}/\text{ndf} = 897.90/6$ for the PL function. The SBPL fit gives $\Phi_0 = (2.82 \pm 0.01) \times 10^{-9}$ m^{-2} sr^{-1} s^{-1} GeV^{-1}, $E_b = 166 \pm 8$ TeV, $\gamma_1 = -3.12 \pm 0.02$, $\gamma_2 = -2.56 \pm 0.02$, and $w = 0.22 \pm 0.06$ with a
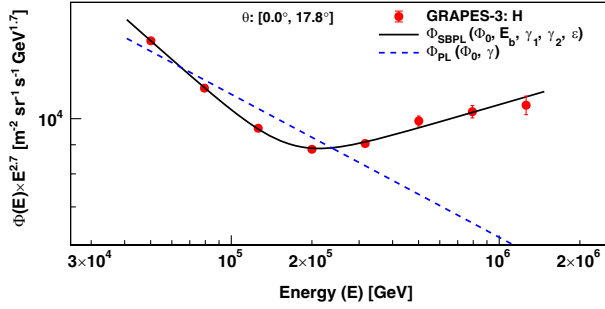
FIG. 5. The GRAPES-3 proton energy spectrum (red markers) fitted with the PL [Eq. (4)] and SBPL [Eq. (5)], represented by the blue dashed line and black line, respectively.

$\chi^2_{\text{SBPL}}/\text{ndf} = 3.36/3$. The improvement in the fit result using the SBPL function with respect to the PL function was quantified by the difference in the χ^2 obtained in both cases, as $\Delta\chi^2 = \chi^2_{\text{PL}} - \chi^2_{\text{SBPL}}$. The χ^2 is reduced by 894.54 for increasing three more free parameters, leading to a significance of 29.7σ. Considering both statistical and systematic uncertainties in the fit, the calculated significance is 3.2σ with a break at energy 164 ± 55 TeV and spectral indices are -3.10 ± 0.19 and -2.59 ± 0.09 before and after, respectively. An independent measurement of the proton + Helium spectrum up to 316 TeV by DAMPE (a direct experiment) suggests a hardening at ~150 TeV [43]. The observed spectral break contradicts the description of the CR spectrum with a single power law up to the Knee and requires more complex models, such as those where multiple classes of sources with different rigidity cutoffs contribute to the flux [14,15].

---

[*]pkm@tifr.res.in

[1] R. L. Workman *et al.* (Particle Data Group), Review of particle physics, Prog. Theor. Exp. Phys. **2022**, 083C01 (2022).

[2] T. Antoni *et al.*, KASCADE measurements of energy spectra for elemental groups of cosmic rays: Results and open problems, Astropart. Phys. **24**, 1 (2005).

[3] M. G. Aartsen *et al.*, Cosmic ray spectrum from 250 TeV to 10 PeV using IceTop, Phys. Rev. D **102**, 122001 (2020).

[4] R. U. Abbasi *et al.*, The energy spectrum of cosmic rays above $10^{17.2}$ eV measured by the fluorescence detectors of the Telescope Array experiment in seven years, Astropart. Phys. **80**, 131 (2016).

[5] A. Aab *et al.*, Measurement of the cosmic-ray energy spectrum above 2.5×10^{18} eV using the Pierre Auger Observatory, Phys. Rev. D **102**, 062005 (2020).

[6] R. U. Abbasi *et al.*, First observation of the Greisen-Zatsepin-Kuzmin suppression, Phys. Rev. Lett. **100**, 101101 (2008).

[7] O. Adriani *et al.*, PAMELA measurements of cosmic-ray proton and helium spectra, Science **332**, 69 (2011).

[8] M. Aguilar *et al.*, Precision measurement of the proton flux in primary cosmic rays from rigidity 1 GV to 1.8 TV with the Alpha Magnetic Spectrometer on the International Space Station, Phys. Rev. Lett. **114**, 171103 (2015).

[9] Q. An *et al.*, Measurement of the cosmic ray proton spectrum from 40 GeV to 100 TeV with the DAMPE satellite, Sci. Adv. **5**, eaax3793 (2019).

[10] O. Adriani *et al.*, Observation of spectral structures in the flux of cosmic-ray protons from 50 GeV to 60 TeV with the Calorimetric Electron Telescope on the International Space Station, Phys. Rev. Lett. **129**, 101102 (2022).

[11] G. H. Choi *et al.*, Measurement of high-energy cosmic-ray proton spectrum from the ISS-CREAM Experiment, Astrophys. J. **940**, 107 (2022).

[12] V. Grebenyuk *et al.*, Energy spectra of abundant cosmic-ray nuclei in the NUCLEON experiment, Adv. Space Res. **64**, 2546 (2019).

[13] P. Lipari and S. Vernetto, The shape of the cosmic ray proton spectrum, Astropart. Phys. **120**, 102441 (2020).

[14] V. I. Zatsepin and N. V. Sokolskaya, Three component model of cosmic ray spectra from 10 GeV to 100 PeV, Astron. Astrophys. **458**, 1 (2006).

[15] T. K. Gaisser, T. Stanev, and S. Tilav, Cosmic ray energy spectrum from measurements of air showers, Front. Phys. **8**, 748 (2013).

[16] S. K. Gupta *et al.*, GRAPES-3-A high-density air shower array for studies on the structure in the cosmic-ray energy spectrum near the knee, Nucl. Instrum. Methods Phys. Res., Sect. A **540**, 311 (2005).

[17] P. K. Mohanty *et al.*, Measurement of some EAS properties using new scintillator detectors developed for the GRAPES-3 experiment, Astropart. Phys. **31**, 24 (2009).

[18] Y. Hayashi *et al.*, A large area muon tracking detector for ultra-high energy cosmic ray astrophysics-the GRAPES-3 experiment, Nucl. Instrum. Methods Phys. Res., Sect. A **545**, 643 (2005).

[19] K. Kamata and J. Nishimura, The lateral and the angular structure functions of electron showers, Prog. Theor. Phys. Suppl. **6**, 93 (1958).

[20] K. Greisen, Cosmic ray showers, Annu. Rev. Nucl. Sci. **10**, 63 (1960).

[21] H. Tanaka *et al.*, Studies of the energy spectrum and composition of the primary cosmic rays at 100–1000 TeV from the GRAPES-3 experiment, J. Phys. G **39**, 025201 (2012).

[22] V. B. Jhansi *et al.*, The angular resolution of GRAPES-3 EAS array after improved timing and shower front curvature correction based on age and size, J. Cosmol. Astropart. Phys. 7 (2020) 024.

[23] F. Varsi *et al.*, A GEANT4 based simulation framework for the large area muon telescope of the GRAPES-3 experiment, J. Instrum. **18**, P03046 (2023).

[24] D. Heck, J. Knapp, J. N. Capdevielle, G. Schatz, and T. Thouw, CORSIKA: A Monte Carlo code to simulate extensive air showers, Forschungszentrum Karlsruhe, Wissenhaltliche Berichte, Karlsruhe, Germany, Report No. FZKA 6019, 1998.

[25] S. Ostapchenko, Monte Carlo treatment of hadronic interactions in enhanced Pomeron scheme: QGSJET-II model, Phys. Rev. D **83**, 014018 (2011).

[26] G. Battistoni *et al.*, Overview of the FLUKA code, Ann. Nucl. Energy **82**, 10 (2015).

[27] S. Agostinelli *et al.*, GEANT4—a simulation toolkit, Nucl. Instrum. Methods Phys. Res., Sect. A **506**, 250 (2003).

[28] T. K. Gaisser, Spectrum of cosmic-ray nucleons, kaon production, and the atmospheric muon charge ratio, Astropart. Phys. **35**, 801 (2012).

[29] See Supplemental Material at http://link.aps.org/supplemental/10.1103/PhysRevLett.132.051002 for details of the data analysis, including MC simulations, the unfolding procedure for estimation of proton composition and spectrum with supporting figures and tables, and comparison of previous and new results, as well as the description of the detailed calculation of systematic uncertainties, which includes Refs. [30–32].

[30] G. Cowan, *Statistical Data Analysis* (Clarendon Press, Oxford, 1998).

[31] D. Fuehrmann, KASCADE-grande measurements of energy spectra for elemental groups of cosmic rays, Ph.D. thesis, University of Wuppertal, 2012.

[32] T. K. Gaisser, R. Engel, and E. Resconi, *Cosmic Rays and Particle Physics* (Cambridge University Press, Cambridge, 2016).

[33] F. Varsi *et al.*, Cosmic ray energy spectrum and composition measurements from the GRAPES-3 experiment: Latest results, Proc. Sci. ICRC2021 (**2021**), 388.

[34] R. Gold, An iterative unfolding method for response matrices, Argonne National Laboratory, USA, Report No. ANL-6984, 1964.

[35] G. D'Agostini, A multidimensional unfolding method based on Bayes' theorem, Nucl. Instrum. Methods Phys. Res., Sect. A **362**, 487 (1995).

[36] J. Friedman, Data analysis techniques for high energy particle physics, *Proceedings of the 3rd CERN School of Computing, Norway*, (CERN, Geneva, 1974), p. 271.

[37] R. Brun and F. Rademakers, ROOT—An object oriented data analysis framework, Nucl. Instrum. Methods Phys. Res., Sect. A **389**, 81 (1997).

[38] A. D. Panov *et al.*, Energy spectra of abundant nuclei of primary cosmic rays from the data of ATIC-2 experiment: Final results, Bull. Russ. Acad. Sci. Phys. **73**, 564 (2009).

[39] Y. S. Yoon *et al.*, Proton and helium spectra from the CREAM-III Flight, Astrophys. J. **839**, 5 (2017).

[40] W. D. Apel *et al.*, KASCADE-Grande measurements of energy spectra for elemental groups of cosmic rays, Astropart. Phys. **47**, 54 (2013).

[41] M. G. Aartsen *et al.*, Cosmic ray spectrum and composition from PeV to EeV using 3 years of data from IceTop and IceCube, Phys. Rev. D **100**, 082002 (2019).

[42] F. Riehn, R. Engel, A. Fedynitch, T. K. Gaisser, and T. Stanev, Hadronic interaction model SIBYLL2.3d and extensive air showers, Phys. Rev. D **102**, 063002 (2020).

[43] F. Alemanno *et al.*, Measurement of the cosmic $p + He$ energy spectrum from 46 GeV to 316 TeV with the DAMPE space mission, arXiv:2304.00137v4.